Payload twisting dynamics and oscillation suppression of tower cranes during slewing motions

Article *in* Nonlinear Dynamics · October 2019

DOI: 10.1007/s11071-019-05247-4

3 authors, including:

Jie Huang
Beijing Institute of Technology
33 PUBLICATIONS **535** CITATIONS

SEE PROFILE

W.E. Singhose
Georgia Institute of Technology
362 PUBLICATIONS **8,884** CITATIONS

SEE PROFILE

Payload Twisting Dynamics and Oscillation Suppression of Tower Cranes during Slewing Motions

Jiaohui Peng[a], Jie Huang[a*], William Singhose[b]

[a] School of Mechanical Engineering, Beijing Institute of Technology, 100081, China

[b] The George W. Woodruff School of Mechanical Engineering, Georgia Institute of Technology, Atlanta, 30332, USA

* Corresponding author: Tel.: +86 1068915097; E-mail: bit_huangjie@bit.edu.cn (J. Huang)

Abstract

Challenging and dangerous material-handling applications in construction have motivated the study of the dynamics and control of tower cranes. Manipulating tower cranes is difficult while moving large-size payloads because of the inevitable payload swing and twisting about the cables. Although significant work has been directed at reducing the swing of point-mass loads, much less effort has been directed at limiting the payload twisting. A nonlinear dynamic model of tower cranes carrying distributed-mass beams is described. Furthermore, an open-loop control method is proposed to reduce both the swing and twisting of the payloads during slewing motions. Simulations and experiments demonstrate the theoretical dynamic behavior of the model and validate the effectiveness of the proposed control method.

Keywords

Tower crane; distributed-mass payload; twisting; swing; oscillation control.

1 Introduction

Tower cranes are widely used in construction throughout the world. As shown in Fig. 1, such cranes move payloads by slewing a jib about the tower, translating a trolley in and out along the jib, and hoisting a suspension cable. However, payload oscillations caused by motions commanded by the human operator are a major

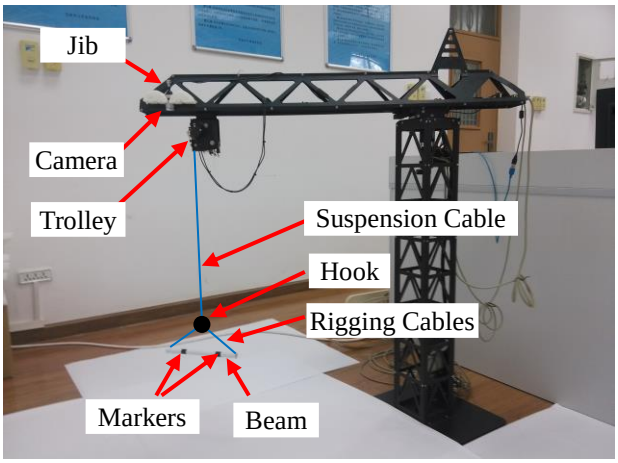

Fig. 1. A small-scale tower crane transporting a distributed-mass beam.

limitation for safe and efficient manipulation. Human operators usually address oscillation problems manually by moving slowly and waiting for unwanted motions to decay.

Bulky payloads are suspended from the hook by rigging cables utilized for transporting large objects. The dynamics of this hoisting mechanism are very complicated because of the payload swing and the payload twisting about the rigging cables. Furthermore, manipulation tasks may be more challenging because the payload twisting cannot be controlled manually, even by skilled operators. Thus, there is a need to study twisting dynamics and control in tower cranes carrying large payloads.

Many researchers have worked on the payload swing dynamics and its control for tower cranes with point-mass payloads [1]. The point-mass payload model cannot capture the payload twisting because the payload size is neglected. The control methods of payload swing dynamics for tower cranes with point-mass payloads include feedback controllers and open-loop controllers. Feedback control methods measure or estimate the payload swing to reduce oscillations in a closed loop, including gain-scheduled control [2-3], fuzzy control [4-5], H_∞ control [6], neural network control [7-8], sliding mode control [9-10], LQR control [11], path-following control [12], adaptive control [13-14], and predictive control [15]. However, accurately sensing the payload swing on-the-fly is challenging [16]. Open-loop

control techniques modify the prescribed commands for swing suppression, including inverse kinematics [17], smooth commands [18], and input shaping [19-22]. However, all the above-mentioned studies have concentrated on tower cranes with point-mass payload dynamics.

The command smoothing technique is also an open-loop controller, which can filter the operator's commands to produce motions that result in minimal oscillations. To suppress the oscillations, the operator command is sent through a smoother to produce a smoothed command, which moves the payload toward the desired positions with low levels of oscillation. The transfer function of one such piecewise smoother is given by [23]:

$$\text{smoother}(s) = \frac{\zeta^2\omega^2}{(1-e^{-2\pi\zeta/\sqrt{1-\zeta^2}})^2} \cdot \frac{(1-e^{-2\pi\zeta/\sqrt{1-\zeta^2}}e^{-2\pi/(\omega\sqrt{1-\zeta^2})\cdot s})^2}{(s+\zeta\omega)^2}, \quad (1)$$

where s is the complex variable of the Laplace transform, ω and ζ are the natural frequency and damping ratio of the payload swing, respectively. The command smoothing technique has been successfully applied to bridge cranes [23-24], slosh suppression [25], a flexible manipulator [26], and a high-speed cam [27].

A previous paper studied payload twisting dynamics in bridge cranes [23]. The modeling and dynamics of bridge cranes transporting distributed-mass payloads were derived. The abovementioned smoother was used to suppress both the payload swing and twisting. Simulations and experiments validate the dynamic behavior and the effectiveness of the method. Of course, the dynamics of the payload twisting of bridge cranes is similar to that of tower cranes during pure radial motions. However, the dynamics of the payload twisting in tower cranes during slewing motions is much more complicated.

The contributions of this paper are the following: 1) This paper presents a model of tower cranes transporting distributed-mass beams. 2) A study of the dynamic behavior of the payload twisting in tower cranes during slewing motions. 3) A demonstration that the smoother described above is also effective on oscillation reduction for these types of cranes.

The rest of this paper is organized as follows. The model of tower cranes

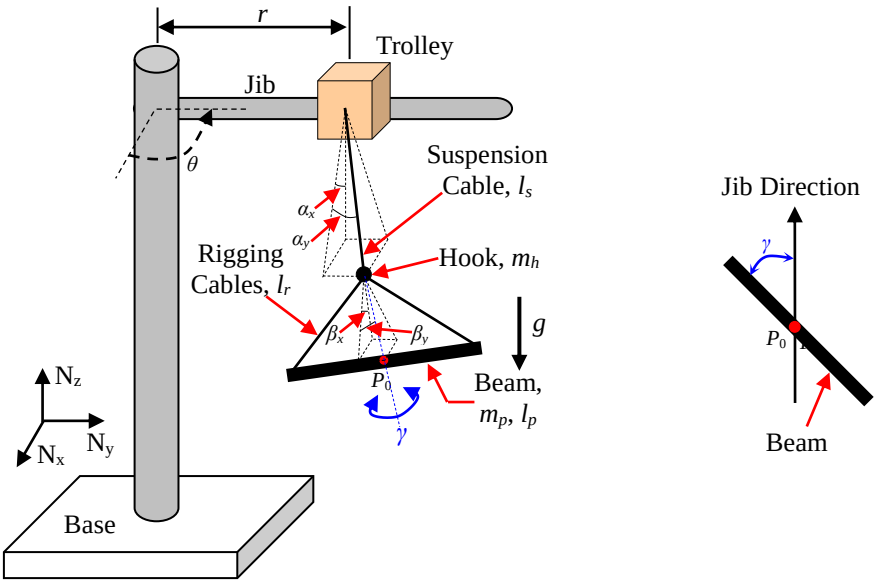

(a) Tower crane side view (b) Twist angle

Fig. 2. Model of a tower crane carrying a distributed-mass beam.

transporting distributed-mass beams is given in Section 2. Then, the dynamics are investigated in Section 3 using both the dynamic model and experimental results. The simulated and experimental results from a small-scale tower crane transporting a distributed-mass beam are used to verify the dynamic behavior and the effectiveness of the control method in Section 4.

2 Modeling

A schematic representation of a tower crane transporting a distributed-mass beam is shown in Fig. 2a. A jib arm of length, L, rotates by an angle of θ about the tower, and a trolley moves radially with a position of r along the jib. A massless suspension cable of length, l_s, hangs below the trolley and supports a hook of mass, m_h. A uniformly distributed-mass beam of mass, m_p, and length, l_p, is attached to the hook by two massless rigging cables of length, l_r. The angle between the radial jib direction and the long axis of the beam is defined as the payload twist angle γ, as shown in Fig. 2b.

It is assumed that the motion of the tower crane is unaffected by motion of the hook and payload due to the high-ratio geared drives and the fact that the effect of

swing is scaled by the sine of the swing angle, which is a very small factor. The model also assumes that the damping ratio is approximately zero, the hook is modeled as a point mass, and the length of the suspension cable does not change during the motions. The inputs to the model are the angular acceleration of the jib, $\ddot{\theta}$, and acceleration of the trolley, $\ddot{r}$. The outputs are the swing angles of the suspension cable α_x and α_y, the swing angles relative to the suspension cable β_x and β_y, and the payload twist angle γ.

Using Kane's method, the nonlinear equations of motion for the model in Fig. 2 were derived. The equations for the swing angles, α_x, α_y, β_x, and β_y, and the payload twist angle γ are:

$$M \cdot \begin{pmatrix} \ddot{\alpha}_x \\ \ddot{\alpha}_y \\ \ddot{\beta}_x \\ \ddot{\beta}_y \\ \ddot{\gamma} \end{pmatrix} + f \begin{pmatrix} \alpha_x, \alpha_y, \beta_x, \beta_y, \gamma, \theta, r, \\ \dot{\alpha}_x, \dot{\alpha}_y, \dot{\beta}_x, \dot{\beta}_y, \dot{\gamma}, \dot{\theta}, \dot{r}, \ddot{\theta}, \ddot{r} \end{pmatrix} = 0, \tag{2}$$

where M is the mass matrix, and f is the column matrix of gravity terms, centrifugal and Coriolis terms, and control input terms. The matrices, M and f, are given in a supplementary downloadable material.

To verify the nonlinear equations of motion shown in (2), a trapezoidal-velocity profile was used to drive both the model (2) and the small-scale tower crane shown in Fig. 1 through a slew of 80 degrees. The jib starts accelerating at time zero, which induces both the payload swing and twisting. Then, the jib decelerates 4 seconds later, which causes additional oscillations. The jib is driven at the maximum slewing speed of 20 %s between the acceleration and deceleration. The experimental and simulated responses of the payload swing are shown in Fig. 3a, while Fig. 3b shows results of the angular velocity, $\dot{\gamma}$, of the payload twist. The payload swing displacement is defined as the position deflection of the mass center of the payload relative to the trolley. The experimental data and the nonlinear simulations show fairly good agreement. The difference between the simulated and experimental results is primarily due to friction and air drag, as revealed by the decay of the experimental response, which is most easily seen in the twist data in Fig. 3b.

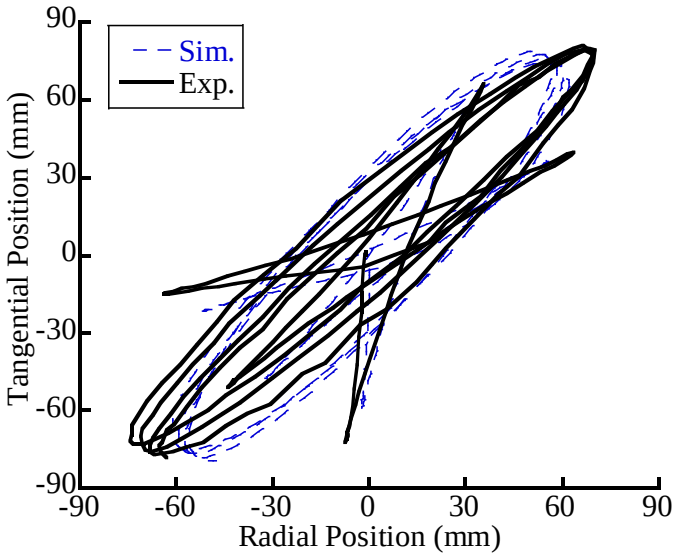

(a) Payload swing viewed from above

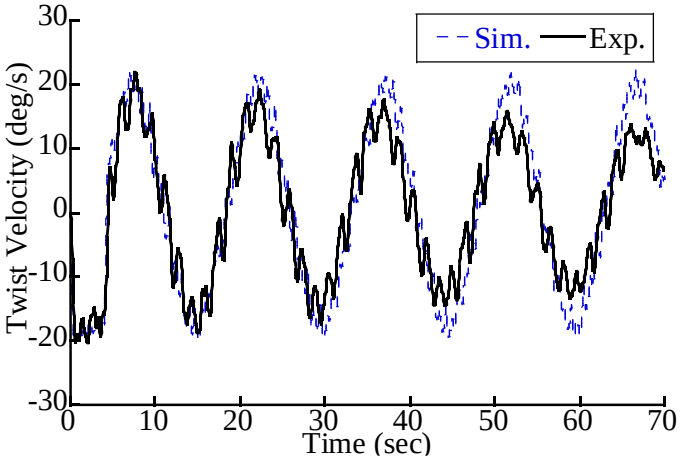

(b) Payload twisting

Fig. 3. Experimental verification of the model.

3 Dynamics

During pure radial motions, the dynamics of tower cranes are similar to that of bridge cranes, which was previously presented in [23-24]. When the initial twist angle is limited to zero, the payload twisting cannot be excited by pure radial motions. Then, the simplified equations during the pure radial motions in this case are given by [24]:

$$\begin{bmatrix} [cR^2 + l_s^2 + c(l_y^2 + l_s^2 + 2l_y l_s \cos(\beta_y))] & c[R^2 + l_y(l_y + l_s \cos(\beta_y))] \\ [R^2 + l_y(l_y + l_s \cos(\beta_y))] & [R^2 + l_y^2] \end{bmatrix} \cdot \begin{pmatrix} \ddot{\alpha}_y \\ \ddot{\beta}_y \end{pmatrix}$$
$$+ \begin{bmatrix} -cl_y l_s \sin(\beta_y) \\ 0 \end{bmatrix} \cdot \dot{\beta}_y^2 + \begin{bmatrix} 0 \\ l_y l_s \sin(\beta_y) \end{bmatrix} \cdot \dot{\alpha}_y^2 + \begin{bmatrix} -2cl_y l_s \sin(\beta_y) \\ 0 \end{bmatrix} \cdot \dot{\alpha}_y \dot{\beta}_y$$
$$+ \begin{bmatrix} l_s(1+c)\sin(\alpha_y) + cl_y \sin(\alpha_y + \beta_y) \\ l_y \sin(\alpha_y + \beta_y) \end{bmatrix} \cdot g + \begin{bmatrix} [l_s \cos(\alpha_y) + cl_s \cos(\alpha_y) + cl_y \cos(\alpha_y + \beta_y)] \\ [l_y \cos(\alpha_y + \beta_y)] \end{bmatrix} \cdot \ddot{r} = 0 \tag{3}$$

where,

$$R = l_p / (2\sqrt{3}), \tag{4}$$

$$l_y = \sqrt{l_r^2 - 0.25 l_p^2}, \tag{5}$$

g is the gravitational constant, and c is the ratio of the payload mass to the hook mass. By assuming small oscillations around the equilibrium position, a linearized model can be derived from the simplified model (3) to approximate the pure radial motions. The resulting linearized natural frequencies of the payload swing during pure radial motions modeled in (3) are [24]:

$$\omega_{1,2}^2 = \frac{g(c+1)}{2l_s}(u \mp v), \tag{6}$$

where

$$u = \frac{l_y^2 + l_s l_y + R^2}{l_y^2 + (c+1)R^2}, \tag{7}$$

$$v = \sqrt{u^2 - \frac{4l_s l_y}{(c+1)(l_y^2 + (c+1)R^2)}}. \tag{8}$$

Equation (6) can also be used to estimate the natural frequencies of the payload swing during slewing motions. This is because the payload swing exhibits only weakly nonlinear dynamic behavior, especially because tower cranes rotate relatively slowly. The swing frequencies are dependent on the suspension cable length, rigging cable length, payload length, and mass ratio. The cable length, payload size, and mass ratio have greater effects on the second-mode swing frequency, ω_2, than the first-mode swing frequency, ω_1. As cable length increases, the first-mode swing

frequency, ω_1, decreases a small amount, while the second-mode swing frequency, ω_2, decreases sharply. Meanwhile, the mass ratio and payload size only have minor impacts on the first-mode swing frequency, ω_1.

If the hook mass is fixed at zero, then the double-pendulum dynamics in (2) can be simplified as single-pendulum dynamics. The swing angles are also assumed to be small around the equilibrium point. Thus, a simplified model for the twisting dynamics can be derived:

$$\begin{aligned}&\ddot{\gamma}+\left[\alpha_y \sin(2\gamma)+\alpha_x-\alpha_x \cos(2\gamma)\right]\dot{\alpha}_x\dot{\theta}+\left[\alpha_x \sin(2\gamma)-2\alpha_y \sin^2\gamma\right]\dot{\alpha}_y\dot{\theta}\\&+\left[\alpha_x \sin\gamma+\alpha_y \cos\gamma\right]\left[\alpha_y \sin\gamma-\alpha_x \cos\gamma\right]\cdot(\dot{\theta})^2+\ddot{\theta}-\alpha_y\cdot\ddot{\alpha}_x=0\end{aligned} \quad . \tag{9}$$

The twist acceleration depends on slewing motions (external excitation) and payload swing (parametric excitation). In the residual stage (no external excitation) of the response in Fig. 3b, the twisting response is similar to a harmonic motion. The payload twists about the swing direction back and forth because the payload swing causes the twist acceleration. The magnitudes of the twist acceleration depend on the amplitude of the payload swing, while the sign of the twist acceleration is dependent on the payload position. When the payload swing is limited to zero, the twist acceleration is also zero. The inertia effect will spin the payload in one direction under conditions of constant angular velocity of the payload twist.

Figure 4 shows the twist frequency for various amplitudes and first-mode frequency of the payload swing. Note that the amplitude and frequency of the swinging varies independently. The twist frequency is lower than the first-mode swing frequency. Both swing amplitude and frequency have a large influence on the twist frequency. The twist frequency increases with increasing swing amplitude and frequency. This effect can be physically interpreted as the interference between the magnitude and sign of the twist acceleration. When the swing amplitude and frequency increase, the payload rotates faster before changing the sign of the twist acceleration. Moreover, the twist frequency is zero for the case of zero payload swing. This is because zero payload swing results in zero twist acceleration. Therefore, a constant angular velocity of the payload twist will spin the payload in one direction. Thus, decreasing both the amplitude and frequency of the swing will result in

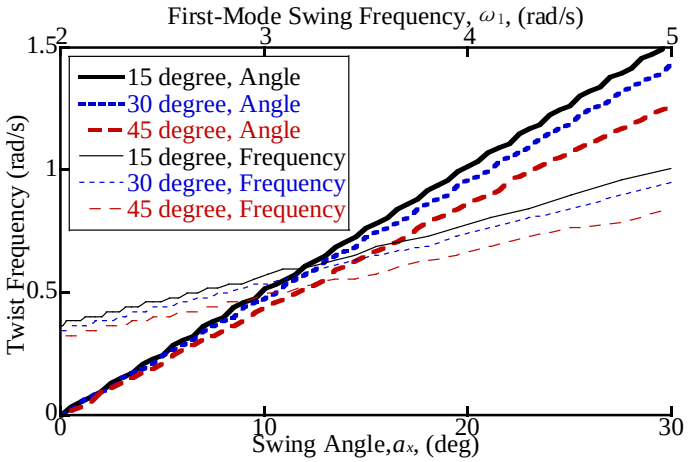

Fig. 4. Twist frequency for various amplitude and first-mode frequency of the swing.

reduction of the twist frequency.

The initial twist angle also has a large impact on the payload twisting dynamics. Figure 4 also shows the payload twisting dynamics for initial twist angles of 15 deg, 30 deg, and 45 deg. The twist frequency decreases as the initial twist angle increases. This effect can also be interpreted as the interference between the magnitude and sign of the twist acceleration. As the initial twist angle increases, the payload rotates further before changing the sign of the twist acceleration. The complex dynamical behavior of the payload twisting is sensitive to the initial twist angle. Thus, the payload twisting exhibits strongly nonlinear dynamical behavior.

4 Experimental Results

The small scale tower crane with distributed-mass beam shown in Fig. 1 was used to verify the dynamical behavior of the model (2) and effectiveness of the smoother (1). The jib arm rotates through a maximum angle of ±155 degrees about the tower. The position of the trolley along the jib was fixed at 75 cm. The jib was driven by a motor with an encoder. A motion control card connected the host computer to the amplifier. A slender beam and a tennis ball served as the payload and hook, respectively. While the mass of the hook was 32 g, the mass and length of the payload were 155 g and 29.7 cm, respectively. The suspension length and rigging cable length were 54 cm and 16 cm, respectively. Both the suspension cable and rigging cables

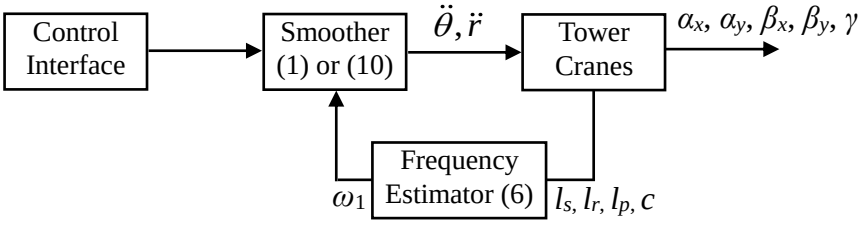

Fig. 5. Control architecture for tower cranes.

were made of Dyneema fishing line.

A camera was mounted on the jib to record the displacements of two markers on the payload. The camera captured video at 30 frames per second. The markers were used to measure the payload swing displacement and twist angle. Averaging the displacements of the two markers was used to represent the payload swing displacement. The twist angular velocity can be calculated by using the inverse tangent function resulting from the two markers.

Figure 5 shows the experimental control architecture. A baseline bang-coast-bang acceleration (trapezoidal-velocity command) is produced via the control interface. The command is then modified by the smoother (1) to create a smoothed command for slewing the jib or moving the trolley. The suspension cable length, l_s, rigging cable length, l_r, payload length, l_p, and mass ratio, c, are used to estimate the design frequency for the smoother by using (6). The first-mode swing frequency, ω_1, is used for the smoother. The design damping ratio is set to zero in the experiments. The smoother for the undamped system is given by:

$$\text{smoother}(s) = \frac{\omega^2}{4\pi^2} \cdot \frac{(1 - e^{-2\pi/\omega \cdot s})^2}{s^2}. \tag{10}$$

An experiment was performed to investigate the effectiveness of the smoother when the jib was slewed 80 degrees using a maximum velocity of 20 deg/s. Figure 6a shows the experimental response of the payload swing caused by the baseline trapezoid and smoothed commands. The residual amplitude is the maximum deflection after the jib stops [24]. The uncontrolled swing had a response with residual amplitudes of 106 mm, while that with the smoother was only 9.9 mm. The

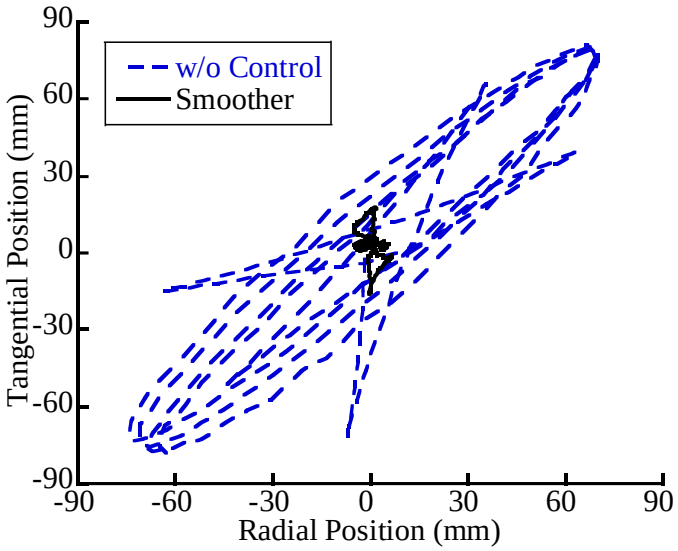

(a) Payload swing viewed from above

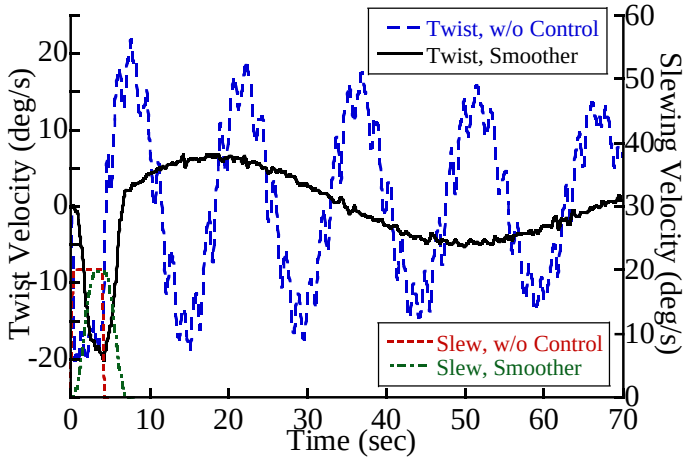

(b) Payload twisting

Fig. 6. Experimental responses for a slewing distance of 80 deg.

slewing velocity profile and the experimental angular velocity of the payload twist are shown in Fig. 6b. The smoothed velocity profile had smooth transitions between boundary conditions, which reduce swing and twisting of the payload. The residual amplitude of the twist angular velocity without the controller was 21.9 deg/s, and that with the smoother was 6.8 deg/s. Additionally, the experimental frequency of large-amplitude low-frequency oscillations in the uncontrolled twisting was 0.43 rad/s, while that with the smoother was only 0.1 rad/s. Thus, the smoother helps reduce the twist frequency. Such a reduction would greatly improve the safety of a real crane moving a heavy payload.

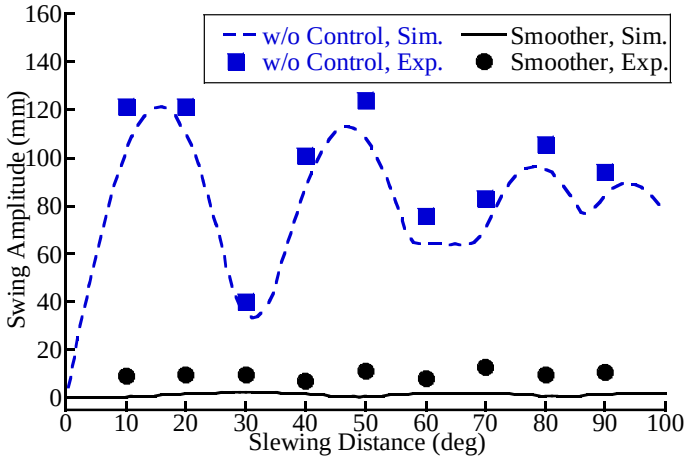

(a) Payload swing

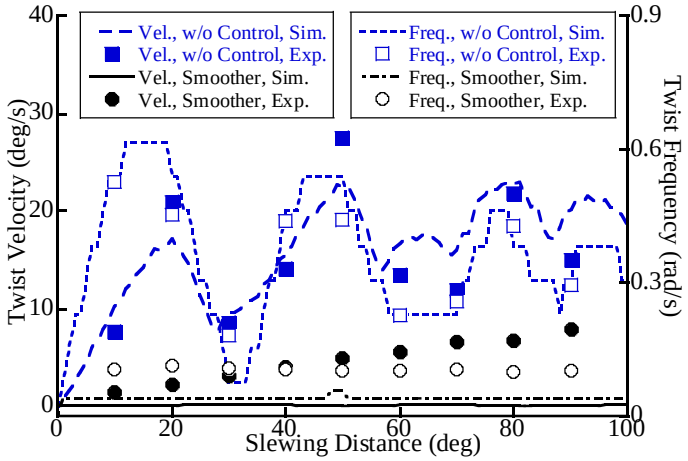

(b) Payload twisting

Fig. 7. Experimental results as a function of slewing distances.

Another experiment was preformed to verify the effectiveness of the smoother for a wide range of slewing motions. The slewing distance ranged from 0 deg to 100 deg. The experimental and simulated results of the residual amplitudes of the payload swing are shown in Fig. 7a. When using the unsmoothed trapezoidal commands, peaks and troughs arose in the amplitude of the payload swing as the slewing distance increased. The design frequency and damping ratio of the smoother were fixed at 4.032 rad/s and 0, respectively. The controlled results were nearly independent of the slewing motions because the smoother eliminated most of the payload swing. The experimental results for the smoother were somewhat worse than the simulated results because of small modeling errors and uncertainty in the overall system.

Figure 7b shows the results of the amplitude and frequency of the payload twisting. The twist frequency was derived by using the fast Fourier transform on both the simulation and experimental data. Peaks and troughs also occurred in both the amplitude and frequency of the payload twisting as the rotating distance changed. When the swing amplitude reached a maximum, the magnitude of the twist acceleration also reached a large value, thereby causing peaks in the twist amplitude and frequency. As predicted, increasing the swing amplitudes induced an increase in the amplitude and frequency of the payload twisting. The experimental data of the controlled twist velocity increased with increasing slewing distances. This is because the model is undamped, while the real system has some small amount of damping. The small damping degrades the oscillation suppression for long slewing distances. However, the experimental results follow the general shape of the simulated curves. The smoother reduced the experimental swing amplitude, twist amplitude, and twist frequency by an average of 89.8%, 71.7%, and 71.0%, respectively. The experimental results verified the simulated dynamical behavior and the effectiveness of the smoother.

The last experiment was performed to study the results from different modeling errors in the frequency, as shown in Fig. 8. Normalized frequency is defined as the ratio of the modeled frequency to the real frequency. Therefore, the normalized frequency is one in the case of a design frequency of 4.032 rad/s. The residual amplitudes of the swing and twisting for the normalized frequency of one were 9.9 mm and 6.8 deg/s, respectively. Note that residual amplitudes of the swing and twisting for the uncontrolled responses were 105.7 mm and 21.9 deg/s, respectively. For the case of the normalized frequency of 0.8 (corresponding to the design frequency of 3.226 rad/s), the residual amplitudes of the swing and twisting were 11.1 mm and 8.0 deg/s, respectively. When the normalized frequency is set to 1.2 (corresponding to the design frequency of 4.839 rad/s), the residual amplitudes of the swing and twisting were 18.6 mm and 8.3 deg/s, respectively. While the residual amplitudes of the swing and twisting for the normalized frequency of 0.6 were 10.1 mm and 7.6 deg/s, those for the normalized frequency of 1.4 were 36.8 mm and 9.0

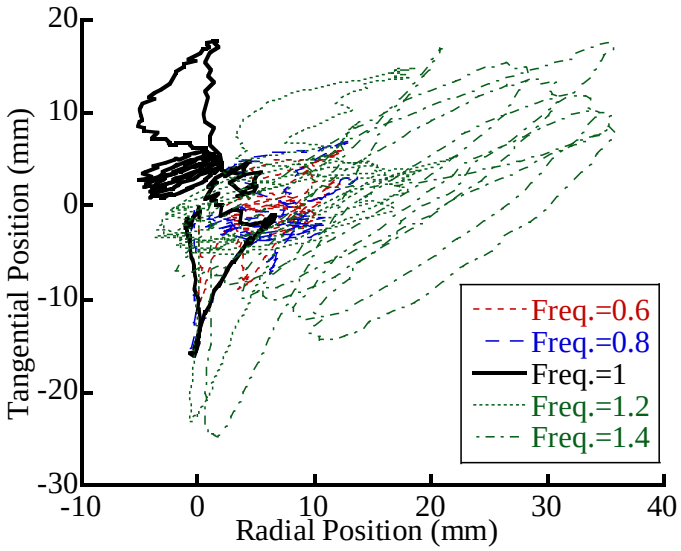

(a) Payload swing viewed from above

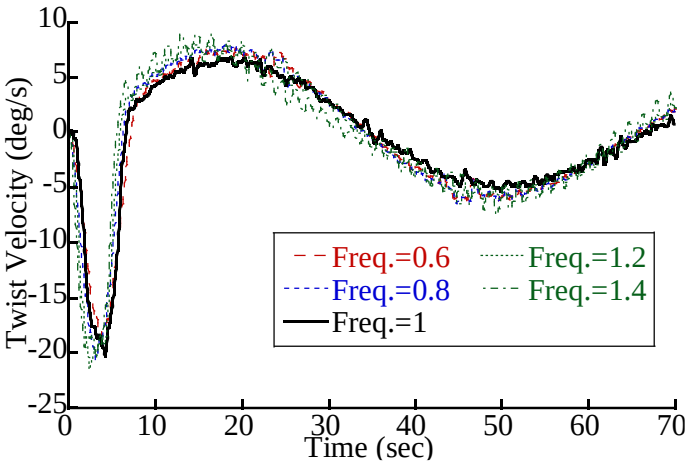

(b) Payload twisting

Fig. 8. Experimental results for various modeling errors in the frequency.

deg/s.

The results clearly show that increasing modeling error increases the payload swing. The payload swing at low normalized frequencies (<1) exhibits insensitivity to the modeling error because of the low-pass filtering effect. The experimental results indicate that the controlled twisting response is insensitive to modeling errors in the frequency. However, the smoother limits both the swing and twisting of the payload to a low level and provides wide robustness to modeling errors in the frequency.

5 Conclusions

A dynamic model of tower cranes transporting distributed-mass payloads was derived. Experimental results verified the model's effectiveness at predicting important effects. The complicated nonlinear dynamics of this system were investigated for a wide range of slewing motions. The proposed command smoother was successful in reducing both the payload swing and twisting. Experimental results from a small-scale tower crane transporting a distributed-mass beam verified the dynamical behavior of the nonlinear model and the effectiveness of the proposed control method.

Declaration of conflicting interests

The authors declare that they have no conflict of interest.

Funding

This study was funded by the National Natural Science Foundation of China under Grant No. 51775041.

References

[1] Hong, K.-S., Shah, U.H.: Dynamics and control of industrial cranes. Springer, Singapore (2019)

[2] Omar, H.M., Nayfeh, A.H.: Gain scheduling feedback control of tower cranes with friction compensation. *Journal of Vibration and Control*. 10(2), 269-289 (2004).

[3] Rauscher, F., Sawodny, O.: An elastic jib model for the slewing control of tower cranes. *IFAC-Papers OnLine*. 50(1), 9796-9801 (2017).

[4] Wu, T.S., Karkoub, M., Yu, W.S., et al.: Anti-sway tracking control of tower cranes with delayed uncertainty using a robust adaptive fuzzy control. *Fuzzy Sets and Systems*. 290(1), 118-137 (2016).

[5] Samin, R.E., Mohamed, Z.: Comparative assessment of anti-sway control strategy for tower crane system. *AIP Conference Proceedings*: *Advances in Electrical and Electronic Engineering: From Theory to Applications*. 1883, 020035-1-9 (2017).

[6] Takagi, K., Nishimura, H.: Control of a jib-type crane mounted on a flexible structure. *IEEE Transactions on Control Systems Technology*. 11(1), 32-42 (2003).

[7] Duong, S.C., Uezato, E., Kinjo, H., et al.: A hybrid evolutionary algorithm for recurrent neural network control of a three-dimensional tower crane. *Automation in Construction*. 23, 55-63 (2012).

[8] Matuško, J., Ileš, Š., Kolonić, F.. et al.: Control of 3D tower crane based on tensor product model transformation with neural friction compensation. *Asian Journal of Control*. 17(2), 443-458 (2015).

[9] Sun, H., Chen, Z., Meng, W.: Fuzzy sliding mode anti-swing control for tower crane base on time-delayed filter. *Chinese Control and Decision Conference*. Taiyuan, China, 2012, pp.2205-2210.

[10] Le, T.A., Dang, V.H., Ko, D.H., et al.: Nonlinear controls of a rotating tower crane in conjunction with trolley motion. *Proceedings of the Institution of Mechanical Engineers, Part I: Journal of Systems and Control Engineering*. 227(5), 451-460 (2013).

[11] Carmona, I.G., Collado, J.: Control of a two wired hammerhead tower crane. *Nonlinear Dynamics*. 84(4), 2137-2148 (2016).

[12] Bock, M., Kugi, A.: Real-time nonlinear model predictive path-following control of a laboratory tower crane. *IEEE Transactions on Control Systems Technology*. 22(4), 1461-1473 (2014).

[13] Le, A.T., Lee, S.G.: 3D cooperative control of tower cranes using robust adaptive techniques. *Journal of the Franklin Institute*. 354(18), 8333-8357 (2017).

[14] Sun, N., Fang, Y., Chen, H., Lu, B., Fu, Y.: Slew/translation positioning and swing suppression for 4-DOF tower cranes with parametric uncertainties: Design and hardware experimentation. *IEEE Transactions on Industrial Electronics*. 63(10), 6407-6418 (2016).

[15] Ileš, Š., Matuško, J., Kolonić, F.: Sequential distributed predictive control of a 3D tower crane. *Control Engineering Practice*. 79, 22-35 (2018).

[16] Wilbanks, J.J., Adams, C.J., Leamy, M.J.: Two-scale command shaping for feedforward control of nonlinear systems. *Nonlinear Dynamics*. 92(3), 885-903 (2018).

[17] Golafshani, A.R., Aplevich, J.D.: Computation of time-optimal trajectories for tower cranes. *IEEE Conference on Control Applications*, Albany, NY, USA, 1995, pp.1134-1139.

[18] Tubaileh, A.: Working time optimal planning of construction site served by a single tower crane. *Journal of Mechanical Science and Technology*. 30(6), 2793-2804 (2016).

[19] Blackburn, D., Singhose, W., Kitchen, J., et al.: Command shaping for nonlinear crane dynamics. *Journal of Vibration and Control*. 16(4), 477-501 (2010).

[20] Lawrence, J., Singhose, W.: Command shaping slewing motions for tower cranes. *Journal of Vibration and Acoustic*. 132, 011002-1-11 (2010).

[21] Vaughan, J., Kim, D., Singhose, W.: Control of tower cranes with double-pendulum payload dynamics. *IEEE Transactions on Control Systems Technology*. 18(6), 1345-1358 (2010).

[22] Elbadawy, A., Shehata, M.: Anti-sway control of marine cranes under the disturbance of a parallel manipulator. *Nonlinear Dynamics*. 82(1-2), 415-434, (2015).

[23] Huang, J., Xie, X., Liang, Z.: Control of bridge cranes with distributed-mass payload dynamics. *IEEE/ASME Transactions on Mechatronics*. 20(1), 481-486 (2015).

[24] Huang, J., Liang, Z., Zang, Q.: Dynamics and swing control of double-pendulum bridge cranes with distributed-mass beams. *Mechanical Systems and Signal Processing*. 54-55, 357-366 (2015).

[25] Huang, J., Zhao,X.: Control of three-dimensional nonlinear slosh in moving rectangular containers. *Transactions of the ASME - Journal of Dynamic Systems, Measurement, and Control*. 140(8), 081016-8 (2018).

[26] Chen, B., Huang, J.: Decreasing infinite-mode vibrations in single-link flexible manipulators by a continuous function. *Proceedings of the Institution of Mechanical Engineers, Part I, Journal of Systems and Control Engineering*. 23(6), 436-446 (2017).

[27] Liang, Z., Huang, J.: Design of high-speed cam profiles for vibration reduction using command smoothing technique. *Proceedings of the Institution of Mechanical Engineers, Part C: Journal of Mechanical Engineering Science*. 228(18), 3322-3328 (2014).